ABSTRACT

XIAOHAI,WAN. Anisotropic Diffusion in Fluorescence Microscopy. (Under the direction of Dr. Sharon R. Lubkin.)

Diffusion of tracer molecules in configurations of collagen fibrils may be used to determine anisotropy of fiber distributions in fluorescence microscopy experiments. Mathematical simulations are used to study the feasibility of these kinds of experiments. The anisotropic diffusion phenomenon can be modeled as a random walk process in simulated completely aligned fibers using the Monte Carlo method. We studied the relationships between the diffusion coefficients (either parallel or perpendicular to fiber orientation) and two influencing factors (density of fibers and relative size of fibers and tracer molecules). Using simulations and statistical analysis, we found that for a given fiber density, relatively bigger size tracer molecules are preferred in order to detect certain level of anisotropy of the fibers. If tracer molecules are too small compared with fibers, even high density of fibers can help little to detect any anisotropy.

NORTH CAROLINA STATE UNIVERSITY

Anisotropic Diffusion in Fluorescence Microscopy

by

Xiaohai Wan

A Thesis Submitted
in Partial Fulfillment of the
Requirements for the Degree

MASTER OF SCIENCE

BIOMATHEMATICS

Approved, Thesis Committee:

Sharon R. Lubkin , Chair
Assistant Professor of Biomathematics

Cavell Brownie
Professor of Statistics

Zhilin Li
Associate Professor of Mathematics

Raleigh, NC

April, 2003

Biography

Born in a small city in P.R.China on January 31, 1976, Xiaohai Wan began his journey in this world. At the age of 18, He went to Beijing, capital of China, to attend Peking University as an undergraduate student. He received 4 years education in computational mathematics and then showed interests in applying mathematics to biological and medical sciences. After graduation, he selected to be a lecturer in Peking University Health Science Center (former Beijing Medical University). He came to North Carolina State University in 2001 to study biomathematics. After he gets his master degree in 2003, he will continue to work for the Ph.D. degree in biomathematics. His career goal is to be a successful biomathematician and biostatistician.

Acknowledgments

I am very thankful to my advisor, Dr. S. R. Lubkin for her kind and indispensable support and guidance. Also, I would like to thank Dr. C. Brownie and Dr. Z.L. Li for insightful suggestions. This work is in part supported by NIH and NSF fundings.

Table of Contents

List of Figures

List of Tables

Chapter 1
Introduction: Anisotropic Diffusion in FRAP

FRAP (Fluorescence Recovery After Photobleaching) techniques can be used to measure the effective diffusion coefficients of tracer molecules within biological materials like articular cartilage [1]. Because of the existence of collagen fibers, molecules' diffusion will be anisotropic, which means that the effective diffusion coefficients for the principal directions of the diffusion tensor may be different. It is known that collagen density and tissue permeability can be determined from diffusion of tracer molecules which may be measured by using FRAP [1]. Experimentalists are now interested in uncovering the relationships between the anisotropic diffusion of molecules and the structural anisotropy of cartilage matrix. Can we feasibly use the same technique to measure collagen anisotropy? Here collagen anisotropy means the axial differences of collagen's 3-dimensional space distribution.

From the continuum perspective, the characteristic equation for the diffusion process without drift can be written as: [2, 3]

$$\frac{\partial C}{\partial t} + (\frac{\partial F_x}{\partial x} + \frac{\partial F_y}{\partial y} + \frac{\partial F_z}{\partial z}) = 0, \tag{1.1}$$

where C is the time dependent concentration (or distribution) of the diffusing substance, and $F_i(i = x, y, z)$ is flux function for specific axis i. In anisotropic media,

the assumptions for the fluxes are:

$$\begin{aligned} -F_x &= D_{xx}\frac{\partial C}{\partial x} + D_{xy}\frac{\partial C}{\partial y} + D_{xz}\frac{\partial C}{\partial z} \\ -F_y &= D_{yx}\frac{\partial C}{\partial x} + D_{yy}\frac{\partial C}{\partial y} + D_{yz}\frac{\partial C}{\partial z} \\ -F_z &= D_{zx}\frac{\partial C}{\partial x} + D_{zy}\frac{\partial C}{\partial y} + D_{zz}\frac{\partial C}{\partial z}, \end{aligned} \tag{1.2}$$

where $D_{ij}(i, j = x, y, z)$ is the diffusion coefficient of the flux function F_i for axis j. If we assume axial independence and that the principal diffusion directions are the same as the coordinate axes, we can write the coefficient matrix $\mathbf{D}$ as

$$\begin{pmatrix} D_x & 0 & 0 \\ 0 & D_y & 0 \\ 0 & 0 & D_z \end{pmatrix} \tag{1.3}$$

Then by plugging the flux functions (1.2) into the characteristic equation (1.1), we can get

$$\frac{\partial C}{\partial t} = \frac{\partial}{\partial x}(D_x\frac{\partial C}{\partial x}) + \frac{\partial}{\partial y}(D_y\frac{\partial C}{\partial y}) + \frac{\partial}{\partial z}(D_z\frac{\partial C}{\partial z}), \tag{1.4}$$

where $D_i(i = x, y, z)$ is the diffusion coefficient for the specific axis i . In our simulations, we assume that the D_is are spatially uniform (not always true), which means that

$$\frac{\partial C}{\partial t} = D_x\frac{\partial^2 C}{\partial x^2} + D_y\frac{\partial^2 C}{\partial y^2} + D_z\frac{\partial^2 C}{\partial z^2}. \tag{1.5}$$

With the particles being dispersed from the origin, the normalized solution to (1.5) using vector-tensor form is [6]

$$C(\mathbf{x_0}, t) = \frac{1}{(2\pi t)^{3/2}\det(2\mathbf{D})^{1/2}} e^{-\frac{1}{2t}\mathbf{x_0}^T(2\mathbf{D})^{-1}\mathbf{x_0}}, \tag{1.6}$$

where $\mathbf{x_0} = (x, y, z)$ is the space coordinate. The level surfaces of this solution are ellipsoids, not spheres, unless the diffusion is isotropic. Experimentally, if we observe elliptical shapes for level surface projections in FRAP, we know that there exist differences among the D's. But the diffusion equation cannot give us the information of the relationships between the D's and the cartilage matrix. Here we are more interested to investigate the relationship between the D's anisotropy and the degree of fiber anisotropy using discretized simulation approach. We hypothesize that the relationship between fiber anisotropy and diffusion anisotropy depends non-trivially on two factors only:

1. Fiber volume fraction (referred to as fiber density, denoted by β).

2. Diameter ratio of fiber and tracer molecules (diameter of fibers is denoted by λ_f, diameter of tracer molecules is denoted by λ_t, and diameter ratio is denoted by $\theta = \frac{\lambda_f}{\lambda_t}$).

In this study, we will examine the relationship between anisotropy of collagen fibers and anisotropy of the tracer molecule diffusion coefficients. For simplicity, we look at the extreme case of complete alignment of infinitely long fibers in the z direction, which means that we have the same configurations for different z values. Typically, dextrans are used as diffusive tracer molecules. Tracer molecules are assumed to be spherical, which is a reasonable assumption for the dextrans used in [1]. Also, all fiber

radii are assumed to be the same and all tracer radii are the same. See Figure 1.1 for an example of part of a configuration. Table 1.1 gives the actual diameters of collagen

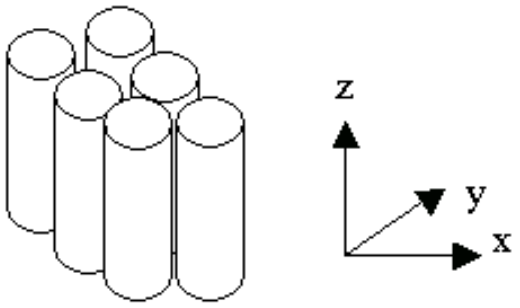

Figure 1.1 Cylinders represent identical collagen fibers which are parallel oriented in the z direction and randomly distributed in the xy plane.

fibrils at different depth in articular cartilage and the size of dextran molecules used in experiments [1]. It can be seen that approximately the diameter ratios for collagen fibrils and dextrans range from 1:2 to 40:1. 9 combinations of fiber and dextran radius are used in the simulations, including 1:2, 2:4, 1:1, 2:2, 2:1, 4:2, 5:1, 10:2 and 10:1. Here 1:2 means that fiber radius is h and dextran (walker) radius is $2h$, where h is the grid length. Other combinations are defined in the same way.

Collagen Fibrils (nm)			Dextrans (nm)			
Surface	Middle	Deep	3kDa	40kDa	70kDa	500kDa
12-25	30-70	80	2.20	4.64	5.51	24.30

Table 1.1 Diameters of collagen fibrils in articular cartilage and dextrans used in FRAP studies.

Chapter 2
Methods

The Monte Carlo method was used to simulate the 3-dimensional anisotropic diffusion of walkers in the fluid between collagen fibers. We discretized the fiber space using rectangular grids. The grid cell length $h = h_x = h_y = h_z$ is chosen to be 1 and is used as the reference value for all the data in the simulation. Given fiber density β, fiber diameter λ_f, and tracer molecule diameter λ_t, 230 fiber configurations which are not totally blocking were generated randomly for each set of 3 parameter values. For each configuration, a Markov Chain model was used to simulate the random walk process for 100 walkers within 800 steps. Squared diffusion distance $d_i^2(n)(i = x, y, z)$ was used to estimate the corresponding D_i using linear regression with respect to time (step) n for each walker. All walkers' $d_i^2(n)$ were averaged to get the pooled estimates of D_i for each configuration. Diffusion coefficient ratios $\gamma_j = \frac{D_j}{D_z}(j = x, y)$ were then calculated to measure fiber anisotropy. Using symmetry we assumed that $D_x = D_y$, so we calculated the diffusion ratio as $\gamma = \frac{(D_x+D_y)/2}{D_z}$. Different estimates of γ for all the 230 configurations were then averaged to get the pooled estimates of γ for same β, λ_f and λ_t. After running the simulations for different sets of β, λ_f and λ_t, the relationship between the estimates of γ and the influencing factors β, λ_f and λ_t were studied using two curve fitting methods with model selection approach.

Also, because the randomly generated configurations may have trapping regions (i.e., extreme cases which restrict the walkers' diffusion from the very beginning), we only used the non-trapping configurations in our simulations to avoid axial bias and also studied the relationship between the probability of generating trapping configurations and the geometric factors.

2.1 Structure of Domain

Samples of tissue are modeled as cubes with all edges' length equal $500h$. Practically, this size is big enough to allow walkers moving within 800 steps without running into the boundary. The origin is set to be in the center of the cube. If there are two "center" grid points (which is our simulated case), the one with smaller grid index is used. Walkers' step length is set to be one grid length h. All walkers start from the origin. Each walker walks on grid points only. Both fibers and walkers are modeled as circles in the xy plane, and are approximated by discretized disks. Examples of disks with different radius are shown in Figure 2.1. Positions of fibers' centers are randomly generated using the uniform random number generator in $MATLAB^{®}$. Fibers are not allowed to form intersections with each other. Fibers are not allowed to intersect the boundaries. A configuration generated will have 0 or 1 for all the grid points. Here 0 means that a grid point is available for walker's moving in; 1 means that a grid point is occupied by the fibers already. Also, notice that walkers have sizes too, so around each fiber, we calculate a boundary layer within which the

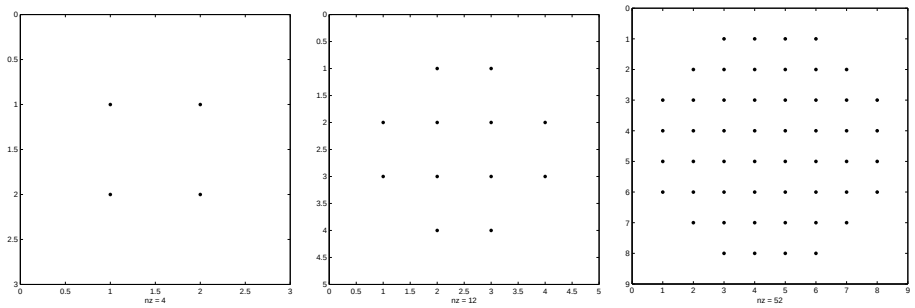

(a) r=1 (b) r=2 (c) r=4

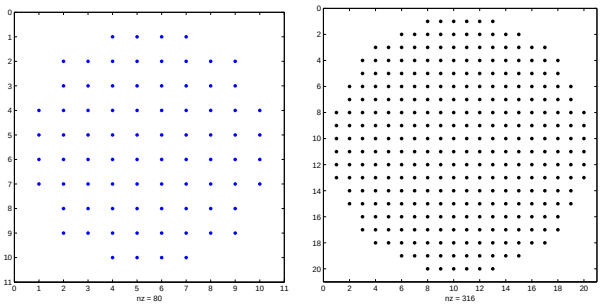

(d) r=5 (e) r=10

Figure 2.1 Discretized disks used to approximate fibers and walkers in simulations.

center of the walker may not penetrate. We also designate the grid points within the boundary layer with 1, then we can track the movement of an equivalent walker with zero radius. The boundary layers of different fibers may overlap with each other. The boundary layers are not allowed to intersect the boundaries either. An example of the randomly generated configurations is shown in Figure 2.2. Because the randomly generated configurations may have trapping zones, which we define as extreme cases when the walker's diffusion is obstructed around the origin, we only use the non-trapping configurations in our simulations to avoid bias of obstruction for either x or y direction.

2.2 Structure of Random Walk

The effects of collagen obstructing dextran diffusion in the xy plane can be illustrated by comparison with free diffusion in the z direction. Diffusion in the z direction is modeled as a simple random walk because there are no obstructions along the z axis. Simple random walk here means that $Pr(Z_{n+1} = Z_n + 1) = Pr(Z_{n+1} = Z_n - 1) = \frac{1}{2}$. A more complicated Markov Chain model is used to simulate the diffusion process in the xy plane, see Figure 2.3. For this Markov Chain model, there are 9 different states. We can number the states from 1 to 9. Every two different states are interconnected with self loop allowed, which means that a walker can go from its current state to any one of the 9 states. The algorithm used for simulation is as follows:

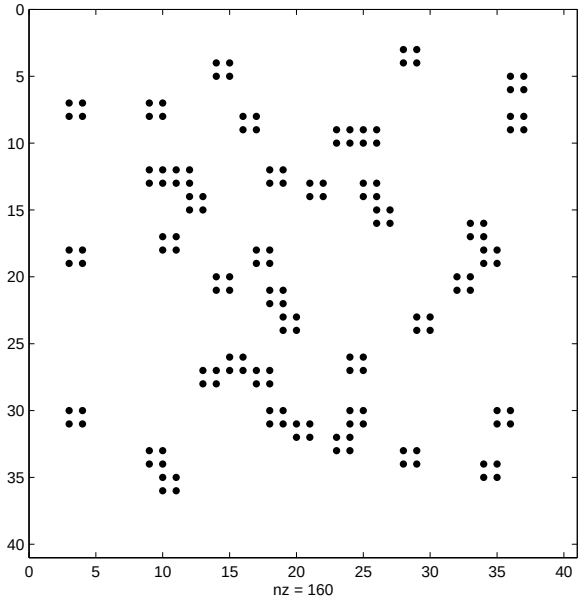

(a)

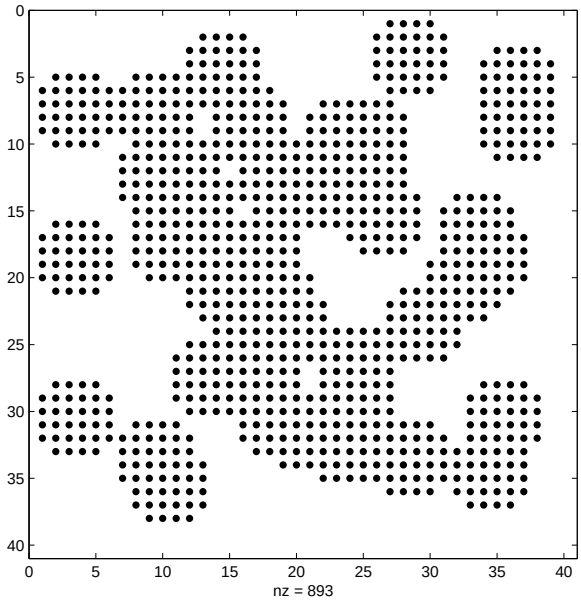

(b)

Figure 2.2 Partial configuration generated in simulations with fiber density being 0.1. (a) A randomly generated fiber configuration with fiber radius 1. (b) Same configuration as in (a) but with buffer for a radius 2 walker.

1 X-1 Y+1	2 X+0 Y+1	3 X+1 Y+1
4 X-1 Y+0	5 X+0 Y+0	6 X+1 Y+0
7 X-1 Y-1	8 X+0 Y-1	9 X+1 Y-1

Figure 2.3 Markov Chain model used in simulations. There are 9 different states in this model. For example, state 5 represents the state in which x and y coordinates remain unchanged; state 3 represents the state in which both x and y coordinates increase by 1.

1. First, generate 3 independent uniform random numbers. Using them to determine the direction of movement for x, y and z axes separately. Let us consider the xy plane first. For example, suppose state 5 is the resting state waiting for transition, and the direction is targeted towards state 2 and state 6 now. See Figure 2.4(a).

2. If site 2, 3, 6 are all obstructed, or only site 3 is obstructed, stay at state 5. See Figure 2.4(b-c).

3. If only site 2 is not obstructed, go to state 2. See Figure 2.4(d).

4. If only site 6 is not obstructed, go to state 6. See Figure 2.4(e).

5. Otherwise, go to state 3. Note that there are 4 different kinds of conditions leading to state 3. See Figure 2.4(f-i).

6. Along the z axis, there are no obstructions, so the walker always moves up or down and never stay still.

In the z direction, walkers can either go up or down; in the x and y direction, walkers can either go forward, backward, or stay still.

2.3 Structure of Simulations

The simulations randomly generate 230 non-trapping fiber configurations for each of 7 selected fiber densities (0.05, 0.10, $\cdots$,0.35) and 9 combinations of fiber and dextran radius (2:4, 1:2, 2:2, 1:1, 4:2, 2:1, 10:2, 5:1 and 10:1). Note that fiber density β is defined as area fraction, which after discretization is point fraction. For one single configuration, total simulation step n is 800 and 100 replications (walkers) are used. Note that if we consider the radius ratio of fiber to walker, we have 5 different ratios: 0.5, 1, 2, 5 and 10. In order to make the data balanced for the ratios, we actually run 2*230=460 non-trapping fiber configurations for the 10:1 case.

2.4 Probability Models and Statistical Methods

A walker's movement in the z direction can be modeled as a simple random walk. The position of the walker after the n_{th} step differs from its position after the $(n-1)_{th}$ step by $\pm h$:

$$z(n) = z(n-1) + \delta_n, \tag{2.1}$$

where $Pr(\delta_n = h) = Pr(\delta_n = -h) = \frac{1}{2}, n \geq 1, z(0) = 0$. So

$$z(n)^2 = z(n-1)^2 + 2z(n-1)\delta_n + \delta_n^2. \tag{2.2}$$

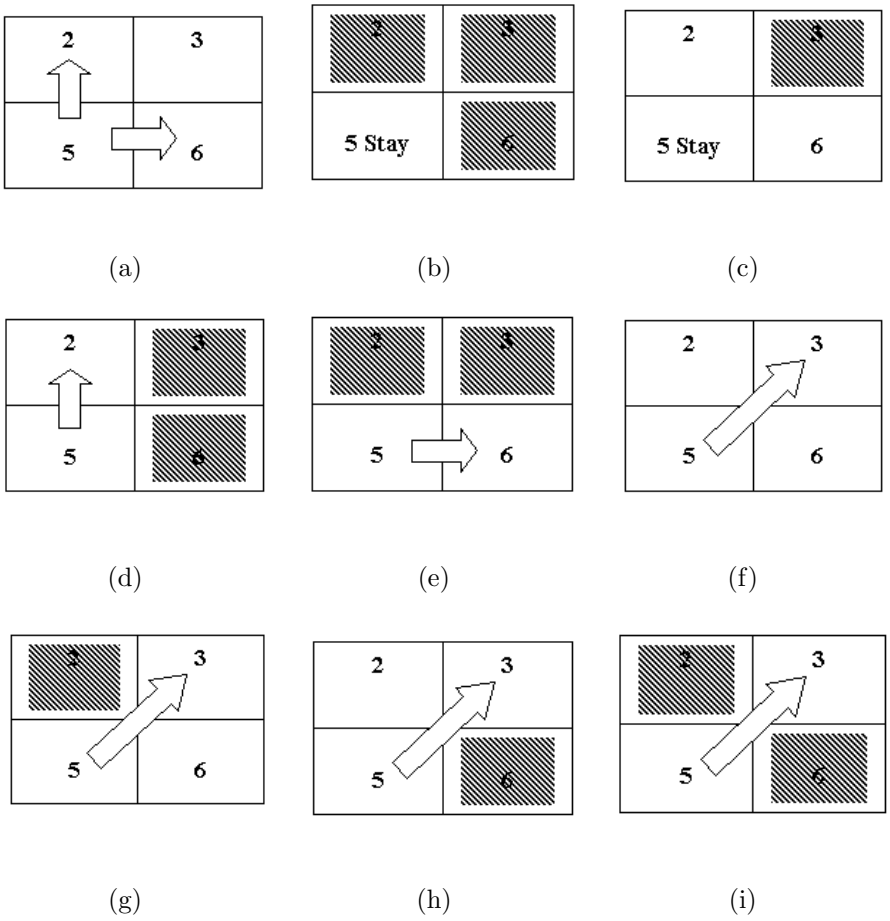

Figure 2.4 Example steps for the Markov Chain model. Dark locations are inaccessible due to fibers and buffer zones. Arrows show the intended (in (a)) or actual moving (in (d)-(i)) direction of a walker. (a) A walker is waiting in state 5 for transition. For both (b) and (c), the walker will stay at state 5. (d) The walker will go to state 2. (e) The walker will go to state 6. For (f), (g), (h) and (i), the walker will go to state 3.

The expectation of $z(n)^2$ is

$$E(z(n)^2) = E(z(n-1)^2) + E(2z(n-1)\delta_n) + E(\delta_n^2) = E(z(n-1)^2) + h^2 \quad (2.3)$$

By induction, we know that [4]

$$E(z(n)^2) = h^2 n = 2D_z n = bn \quad (2.4)$$

where $D_z = \frac{h^2}{2} = \frac{1}{2}$(note that $h = 1$) and b is the regression coefficient. We know that D_z is in fact the diffusion coefficient in equation (1.5) [4]. The squared diffusion distance $d_z^2(n)$ can be used to estimate $E(z(n)^2)$:

$$d_z^2(n) = bn + Y_n, \quad (2.5)$$

where $Y_n = 4h^2(X_n - \frac{n}{2})^2 - h^2 n$ and $X_n = \frac{\sum_{i=1}^{n}(\delta_i + h)}{2h} \sim binomial(n, \frac{1}{2})$. Although Y_n is not to be independent normal error, we can still use ordinary linear regression on $d_z^2(n)$ with step n to estimate D_z. Note that the estimated diffusion coefficient D_z is only half of the linear regression coefficient b. In both x and y directions,we assume that the diffusion also follows equation (2.4), while values of D_x and D_y are now dependent on β, λ_f and λ_t.

In our model, we assume that D_x and D_y have no significant difference averaged over all possible configurations, which means that in the xy plane, the diffusion is isotropic. Although there exist some configurations for which the estimates of D_x and D_y are quite different, these estimates are still kept because we are only interested in the magnitude of D_x and D_y compared with D_z. See Figure 2.5 for an example of regression in x and y direction compared with z direction. As we can notice from the

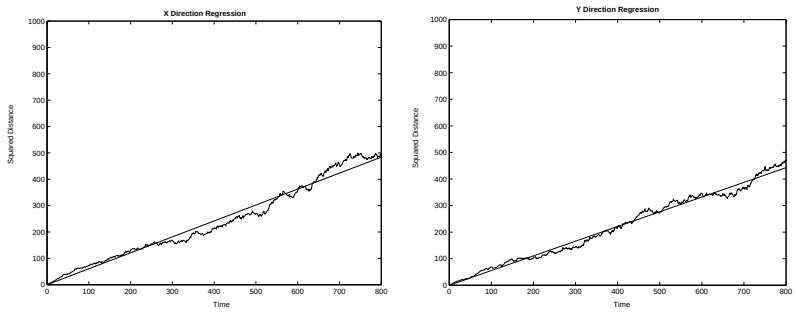

(a) b=0.60

(b) b=0.55

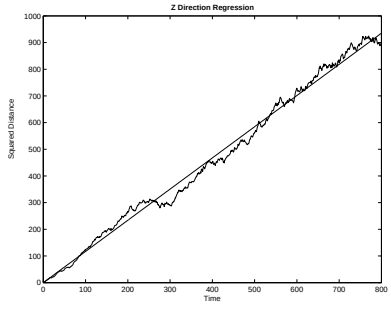

(c) b=1.17

Figure 2.5 Sample output of linear regression in x, y and z directions. The 3 figures are generated in a single simulation using parameters β=0.15, λ_f=2 and λ_t=1. The curve lines are the squared diffusion distance $d_i^2(n)(i = x, y, z)$ and the straight lines are the fitted regression lines. The regression coefficient $b's$ are shown. The dash-dot line in (c) is the theoretical line where $b = 1$. The difference between the sampled b value and the theoretical value 1 is due to the finite grids we used and finite samples.

above output, the estimates of D_x and D_y may be quite different for a single configuration. It happens mainly because of randomly generated configuration bias in either x or y direction. We assume that by averaging the estimates of different randomly generated configurations, this kind of bias can be balanced without influencing the relationship of diffusion coefficients and the factors β, λ_f and λ_t. D_x and D_y are averaged to estimate the diffusion coefficient ratio γ using $\gamma = \frac{(D_x+D_y)/2}{D_z}$.

2.5 Trapping Probability p_t's Estimation

Because the configurations are randomly generated, there could be configurations which have no spanning path to allow walkers to diffuse away starting from the origin, especially for high density of fibers. Percolation theory can be used to study when a fiber configuration is macroscopically open to the diffusion phenomenon [5]. Intuitively, there exists a critical value β_c for fiber density: when fiber density $\beta > \beta_c$, the configurations are macroscopically closed to diffusion; when $\beta < \beta_c$, the configurations are macroscopically open to diffusion. β_c is well below the maximal packing density, which can be calculated as $\frac{\pi}{6} \approx 0.52$. Here we are not interested in finding the critical value β_c, because cartilage fiber density falls below 35% of collagen presumably to stay away from the percolation limit and allow some large molecules to be able to diffuse. However, we still need to consider the microscopic trapping phenomenon. This kind of trapping can make the computation of diffusion coefficients greatly biased for either x or y direction. An arbitrary criterion is used

here to label a configuration as trapping: if after 80 steps (10% of the total steps) of walking, the standard deviation of the walker's diffusion coefficients for either x or y direction is below $0.01h$, then the specific configuration is said to be trapping. Configurations will be continually generated until 230 non-trapping ones are available for diffusion simulations. We define p_t as the probability that a randomly generated configuration is a trapping one, n as the total configurations generated in order to get $m = 230$ non-trapping ones.

Chapter 3
Results

3.1 Diffusion Ratio γ's Dependence on Fiber Density β, Fiber Size λ_f and Walker Size λ_t

We define the diffusion coefficient ratio γ as $\frac{(D_x+D_y)/2}{D_z}$. We also denote fiber density with β, diameter of fibers with λ_f, and diameter of walkers with λ_t. In this study, we want to find the relationship between γ and the influencing factors using the simulated data. See Figure 3.1(a) for γ plotted against different combinations of β, λ_f and λ_t averaged across 230 different configurations. From Figure 3.1(a), we see that it is acceptable that the curves with same fiber-walker radius ratio $\theta = \frac{\lambda_f}{\lambda_t}$ can be grouped together. See Figure 3.1(b) for γ plotted against different fiber/walker size ratio θ averaged across 460 different configurations. We can see that γ decreases as β increases and θ decreases. Also, it shows that for θ =5 and 10, γ curves have relatively bigger estimation error; while for $\theta = 0.5$, γ curve is estimated pretty well.

Two curve fitting models are shown below for the data in Figure 3.1(b).

Model 1: it is intuitively attractive to fit the data in Figure 3.1(b) using an exponential decaying function [7] like $\gamma(\beta, \theta) = (1-\beta^3)e^{\frac{a\beta^{3/2}}{\theta}}$, where a is the parameter to be fitted. Note that we require $a < 0$ since for a given β, as θ increases, γ increases. Also the function satisfies the boundary conditions, namely $\gamma(1, \theta) = 0$ and $\gamma(0, \theta) = 1$. The inverse of γ's standard deviation is used as regression weight.

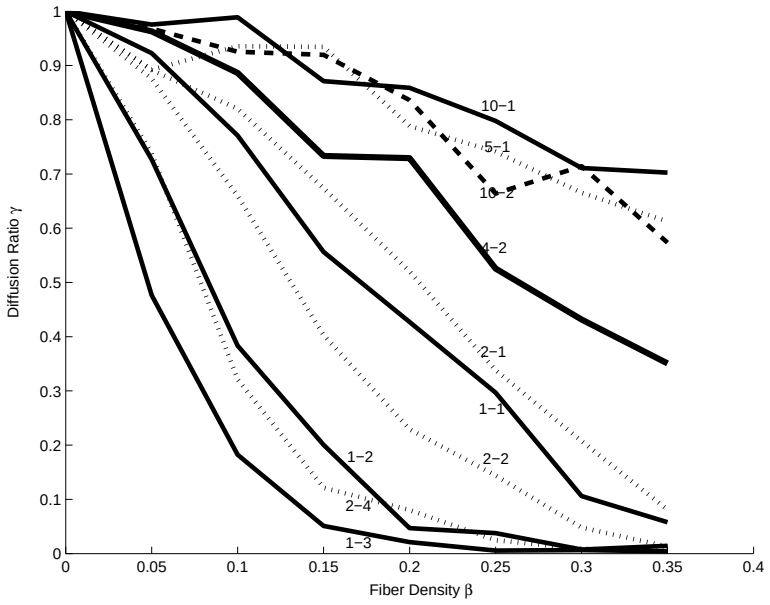

(a)

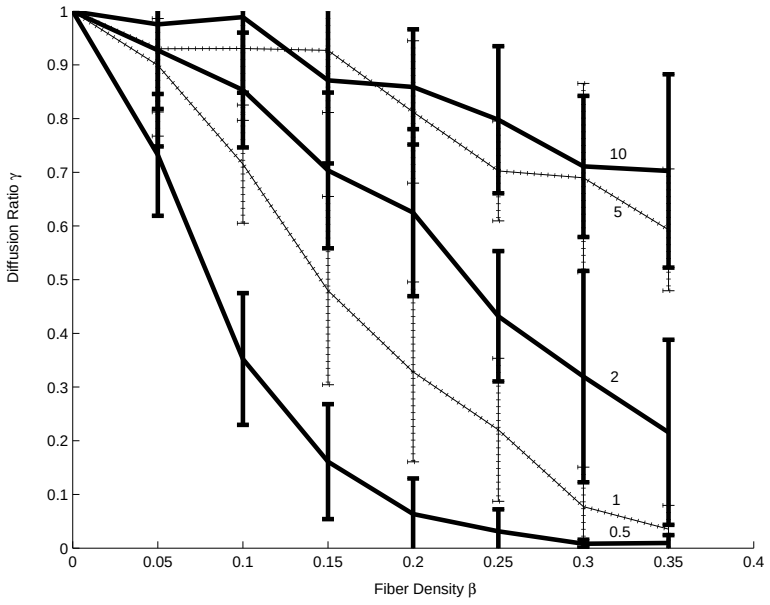

(b)

Figure 3.1 γ plots. (a) γ plotted against different β, λ_f and λ_t. E.g., "10-1" means that λ_f=10 and λ_t=1. For $\beta = 0$ there is only one point which means that the theoretical ratio of an isotropic diffusion would be exactly 1. Also, the ratio of "1-3" is included here for verification only. Note that the replication for each point is 230 except for "1-3" and "10-1", which are 10 and 460 respectively. (b) γ plotted against different $\theta = \frac{\lambda_f}{\lambda_t}$. E.g., "10" means that λ_f=10 and λ_t=1; "5" means that λ_f=10 and λ_t =2 or λ_f=5 and λ_t =1. The standard deviation for each point is also shown.

The fitted a is -13.3 ± 0.4 and $R^2 = 0.89$. If we use unweighted regression, the fitted a is -13.1 ± 0.4 and $R^2 = 0.99$. Only weighted regression results are presented here. See Figure 3.2 for the data with fitted curves residuals. No trends seem to exist for the residuals. Also, the residuals' magnitude is less than 0.08.

Model 2: we can also fit a two-parameter model using $\gamma(\beta, \theta) = (1-\beta^a)e^{(1-e^{(\frac{6\beta^b}{\theta})})}$, where a, b are the parameters to be fitted. Note that the model automatically suffices that given β, as θ increases, γ increases. Also the function satisfies the boundary conditions, namely $\gamma(1, \theta) = 0$ and $\gamma(0, \theta) = 1$. The inverse of γ's standard deviation is still used as regression weight. The fitted a is 1.7 ± 0.1, the fitted b is 1.30 ± 0.02 and $R^2 = 0.92$. If we use unweighted regression, the fitted a is 1.7 ± 0.1, the fitted b is 1.29 ± 0.01 and $R^2 = 0.99$. Only weighted regression results are presented here. See Figure 3.3 for the data with fitted curves and residuals. No trends seem to exist for the residuals. Also, the residuals' magnitude is less than 0.08. It is also interesting that weighted and unweighted regression give almost the same fits.

It is clear that model 2 works better than model 1. We can see that the fittings work much better at high level of density because we have used the inverse of $\gamma's$ standard deviation as the regression weight and the standard deviation is smaller at high β. Experimentally, we are most interested in the cases where fiber density is around 20% and the diffusion ratio is relatively small. Both models presented are reliable to give good predictions for experimental usage.

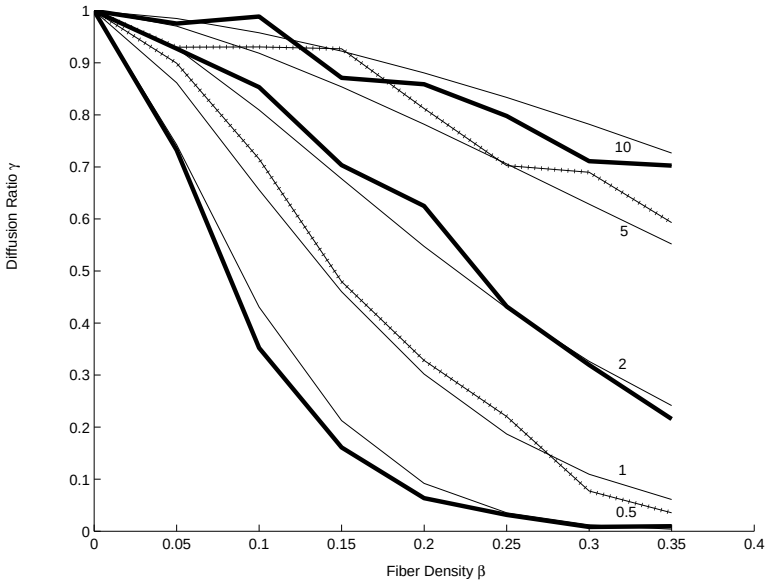

(a)

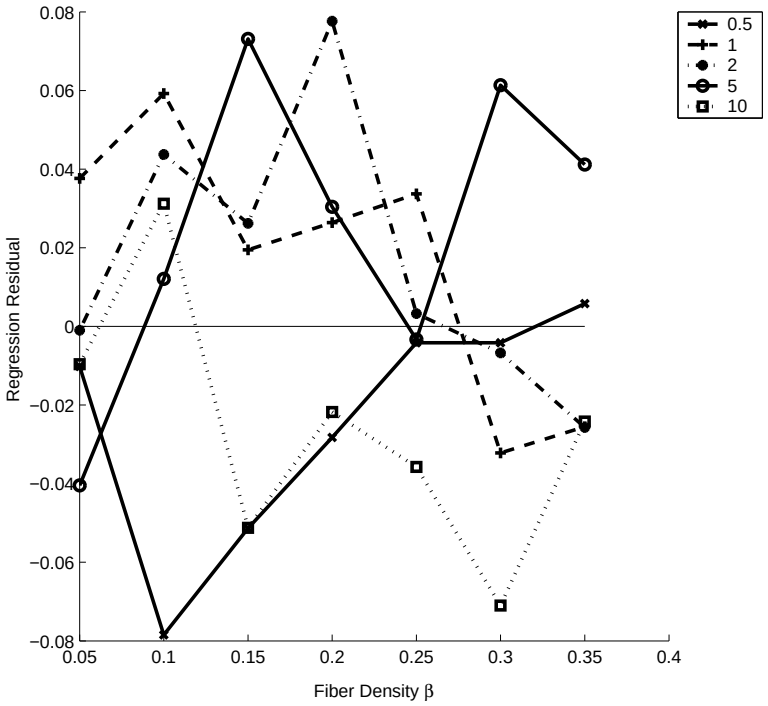

(b)

Figure 3.2 Model 1. $\gamma(\beta, \theta) = (1 - \beta^3)e^{\frac{a\beta^{3/2}}{\theta}}$. (a) Data fitting using model 1. (b) Regression residual.

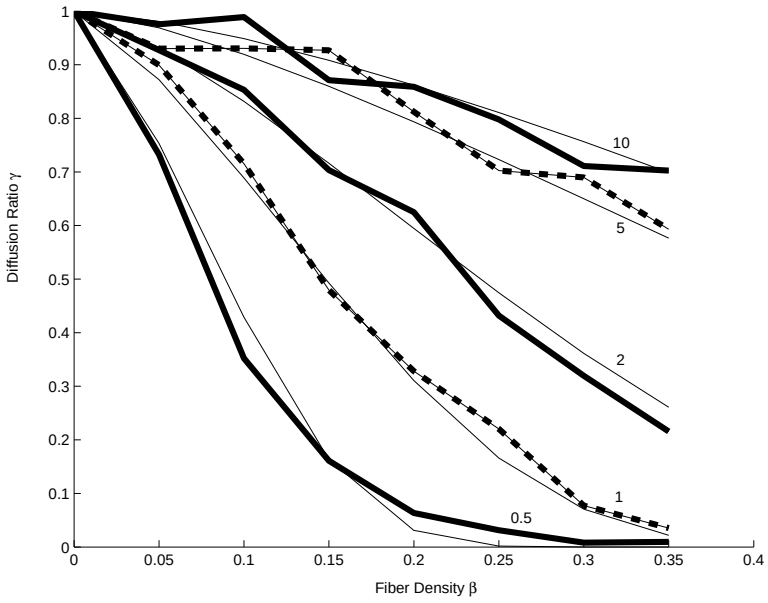

(a)

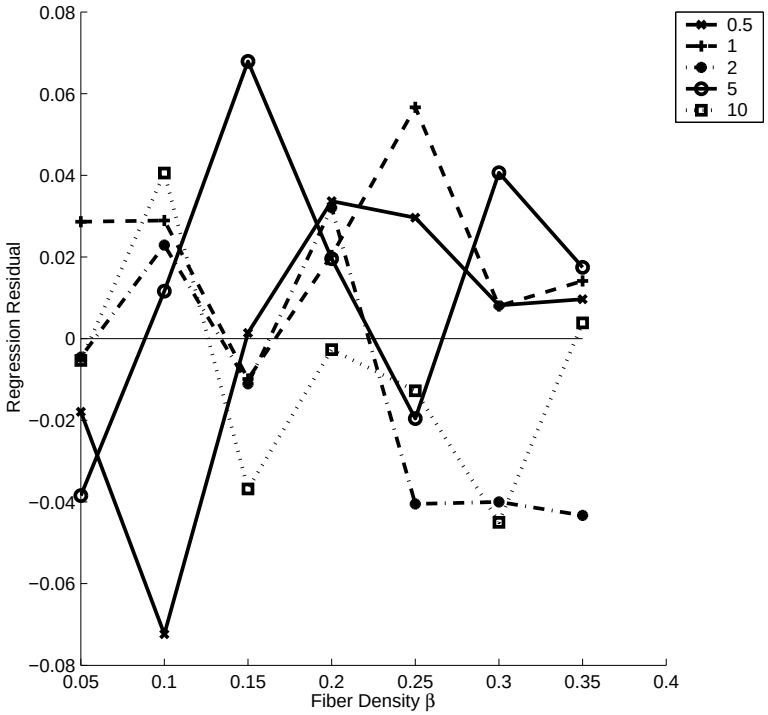

(b)

Figure 3.3 Model 2. $\gamma(\beta, \theta) = (1 - \beta^a)e^{(1-e^{(\frac{6\beta^b}{\theta})})}$. (a) Data fitting using model 2. (b) Regression residual.

3.2 The Estimate of Trapping Probability p_t's Dependence on Fiber Density β, Fiber Size λ_f and Walker Size λ_t

For the trapping probability p_t, let n be the number of total configurations generated in order to get m non-trapping ones. We know that n has a *negative binomial*$(m, 1-p_t)$ distribution. We may conclude that the frequency estimate of p_t is $\frac{n-m}{n}$, which is also the MLE of p_t .

See Figure 3.4 for the estimate of $p_t(\beta)$ averaged across different combinations of λ_f and λ_t. From the figure, we can see that p_t is non-decreasing with β as expected, and the averaged estimation curve has a sigmoid shape. Given a fiber density β, p_t is almost non-increasing for λ_f, which means that fibers with bigger sizes make diffusion easier. Also, given a fiber density β, p_t is non-decreasing for λ_t, which means that tracer molecules with smaller sizes make diffusion easier. Approximately, β_c is about 0.50 for our model when the trapping probability p_t is almost 1 for all combinations.

3.3 Discussion

It is quite clear that the diffusion ratio γ decreases as fiber density β increases. Also, for a specific fiber density, the curves increase as θ increases. This means that the relatively larger tracer molecules are preferred for detecting fiber anisotropy, which is consistent with the results of hindered diffusion in porous materials [8]. As we have seen, our regression models give satisfactory outcomes for fitting the simulated data. Although model 2 gives a little better fitting ($R^2 = 0.92$ versus 0.89), we

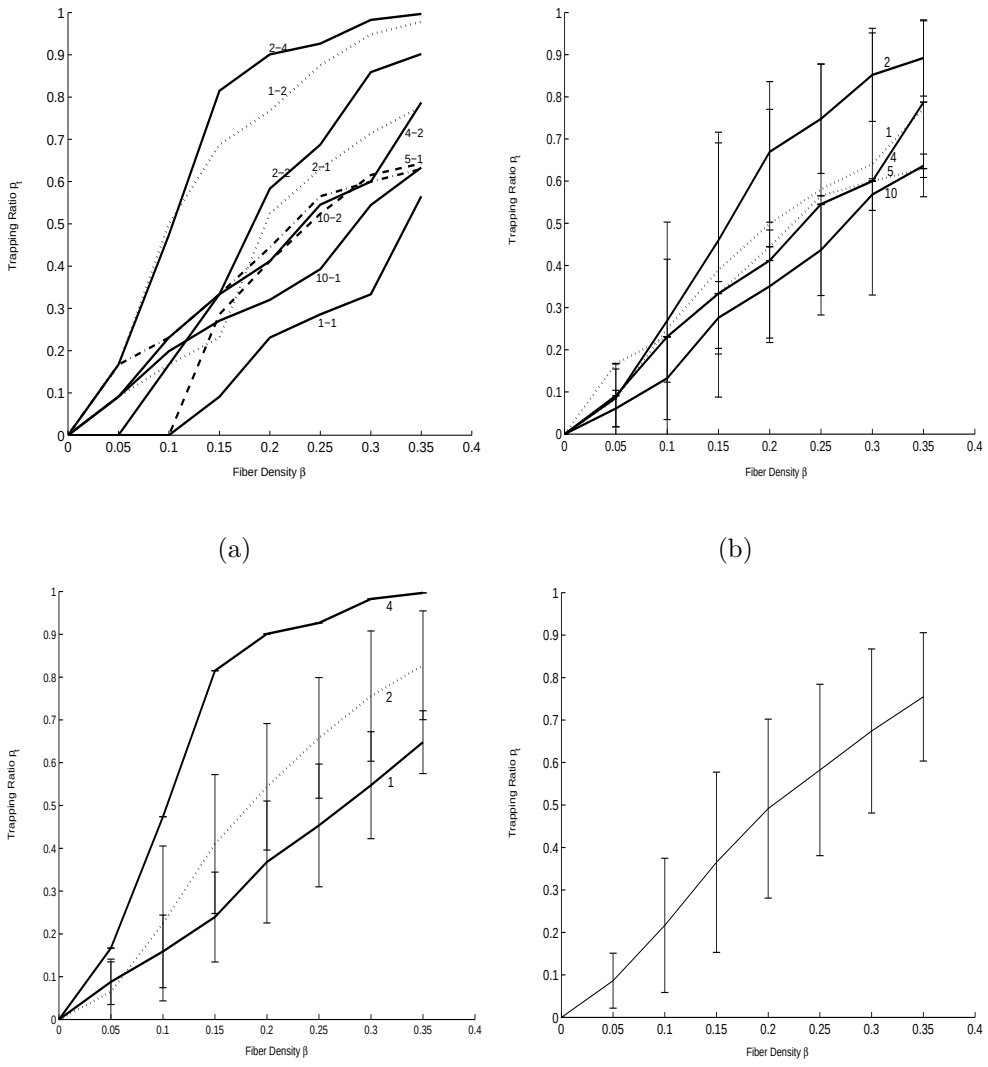

(a) (b)

(c) (d)

Figure 3.4 The estimates of p_t. (a) The estimate of p_t against 9 combinations of λ_f and λ_t. (b) The estimate of p_t averaged across same λ_f. (c) The estimate of p_t averaged across same λ_t. (d) The estimate of p_t averaged across combinations of λ_f and λ_t against β.

would prefer model 1 to be used instead because of parsimony and simplicity factors. Numerically, both models are good enough to be used for pre-experiment prediction and post-experiment validation. The simulated relationship between γ and β, θ can be used to give approximated size information for choosing different dextrans. For instance, if the cartilage is 20% collagen and the experimenters want to be able to detect anisotropy with $\gamma = 0.3$, they should make sure to use a dextran of at least the diameter of the fibers. If they need a γ of 0.1, they would need to use a dextran twice as big as the fiber diameter at 20% collagen density. We can also use the simulated results to validate (or invalidate) the experimental outcomes.

The simulations used here neglect molecule-molecule interactions, so the results may be accurate only for tracer molecules of low density [8]. Also, in articular cartilage, other biological molecules may also influence the diffusion of tracer molecules of interest.

References

1. Leddy, H.A. and F. Guilak, "Diffusion Coefficients Vary with Depth in Articular Cartilage", Annals of Biomedical Engineering 29(S1): S30, 2001.

2. J.Crank, *The Mathematics of Diffusion*. Clarendon Press, Oxford: 1956.

3. H.S.Carslaw., J.C.Jaeger, *Conduction of Heat in Solids*. Clarendon Press, Oxford: 1959.

4. Howard C. Berg, *Random Walks in Biology*. Princeton University Press, Princeton, N.J.: 1983.

5. Muhammad Sahimi, *Applications of Percolation Theory*. Taylor & Francis, London; Bristol, PA : 1994.

6. Anders Stockmarr, "The Distribution of Particles in the Plane Dispersed by a Simple 3-dimensional Diffusion Process", J.Math.Biol. 45, 461-469, 2002.

7. Samiul Amin, "Brownian Motion in Viscoelastic Media", Thesis (Ph.D.), North Carolina State University, 2002.

8. Deen WM, "Hindered Transport of Large Molecules in Liquid-Filled Pores", AIChE Journal 33:1409-1425, 1987.